Cation distribution in the $Bi_{4-x}RE_xTi_3O_{12}$ (RE = La, Nd) solid solution and Curie temperature dependence

J. Arreguín-Zavala[a,*], *M.E. Villafuerte-Castrejón*[a,1], *F. González*[a], *L. Bucio*[b], *O. Novelo-Peralta*[a], *R.Y. Sato-Berrú*[c], *J. Ocotlán-Flores*[c]

[a]*Instituto de Investigaciones en Materiales, Universidad Nacional Autónoma de México, Ciudad Universitaria, A.P. 70-360, 04510 México D. F., Mexico*
[b]*Instituto de Física, Universidad Nacional Autónoma de México, Ciudad Universitaria, A.P. 20-364, 01000 México D. F., Mexico*
[c]*Centro de Ciencias Aplicadas y Desarrollo Tecnológico, Universidad Nacional Autónoma de México, Ciudad Universitaria, AP 70-186, México D. F, Mexico*

ARTICLE DATA

Article history:
Received 30 April 2008
Received in revised form
4 September 2008
Accepted 5 September 2008

Keywords:
Co-precipitation method
Doping effect
Curie temperature
Raman spectroscopy
Aurivillius phase

ABSTRACT

$Bi_{4-x}RE_xTi_3O_{12}$ (RE = La, Nd) ferroelectric powders were prepared by a co-precipitation route. Raman spectroscopy and X-ray diffraction were employed to determine the crystal site of La^{3+} and Nd^{3+} as well as the effect of their addition on the crystal structure. It was found that La atoms were not only placed preferentially in pseudo-perovskite A sites for concentrations $x \leq 1.2$ but also substituted for Bi^{3+} in $(Bi_2O_2)^{2+}$ layers for greater concentrations. A similar behavior was observed with the limit value $x = 0.8$ in case of Nd^{3+}. In solid solution La or Nd^{3+} ions diminish the distortions in the octahedron formed by oxygen atoms, so there is a tendency to undergo a transition in crystal symmetry from orthorhombic to tetragonal. Finally differential scanning calorimetry (DSC) shows a linear dependence of the Curie temperature (T_c) when the amount of La^{3+} or Nd^{3+} was increased.

© 2008 Published by Elsevier Inc.

1. Introduction

The Aurivillius phases were first described in 1949 [1]. These phases consist of $(A_{n-1}B_nO_{3n+1})^{2-}$ blocks regularly interleaved with $(Bi_2O_2)^{2+}$ sheets. For $n = 3$, $Bi_4Ti_3O_{12}$ Bismuth Titanate (BIT) undergoes a ferroelectric to paraelectric phase transition at the Curie temperature ($T_c = 675$ °C). The room-temperature diffraction data can be accounted for by orthorhombic symmetry (B2cb) with $a = 5.4489$ Å, $b = 5.41$ Å, and $c = 32.815$ Å [2].

Compared to other ferroelectric materials [e.g. lead zirconate titanate (PZT) can be employed in the range of 0–250 °C], this compound has a high Curie temperature (T_c) which makes it useful over a wide temperature range for standard electronic elements (sensors, capacitors and piezoelectric transducers). From consideration of the structural chemistry of the Aurivillius phases, the compositional modification as well as the size effect can offer useful guidelines toward the search for the new materials, which can meet the commercial demands for T_c, conductivity, coercivity and compliance [3].

The ion substitution, also known as site engineering technique [4], may be an effective method for improving the ferroelectric properties of BIT crystals. In this regard, La^{3+}, Nd^{3+}, substituted materials have recently proven very attractive due to their large ferroelectricity and their excellent fatigue resistance [5–7]. This large ferroelectricity as well as a low leakage current density can be explained by the rotation enhancement of TiO_6 octahedra in the *a–b* plane accompanied with a shift of the octahedron along the *a*-axis by the La^{3+} substitution for Bi^{3+}

* *Corresponding author*. Tel.: +52 55 56224646; fax: +52 55 56161371.
E-mail address: javoaz@yahoo.com.mx (J. Arreguín-Zavala).
[1] On sabbatical leave in Facultad de Química, Universidad Complutense de Madrid.

1044-5803/$ – see front matter © 2008 Published by Elsevier Inc.
doi:10.1016/j.matchar.2008.09.003

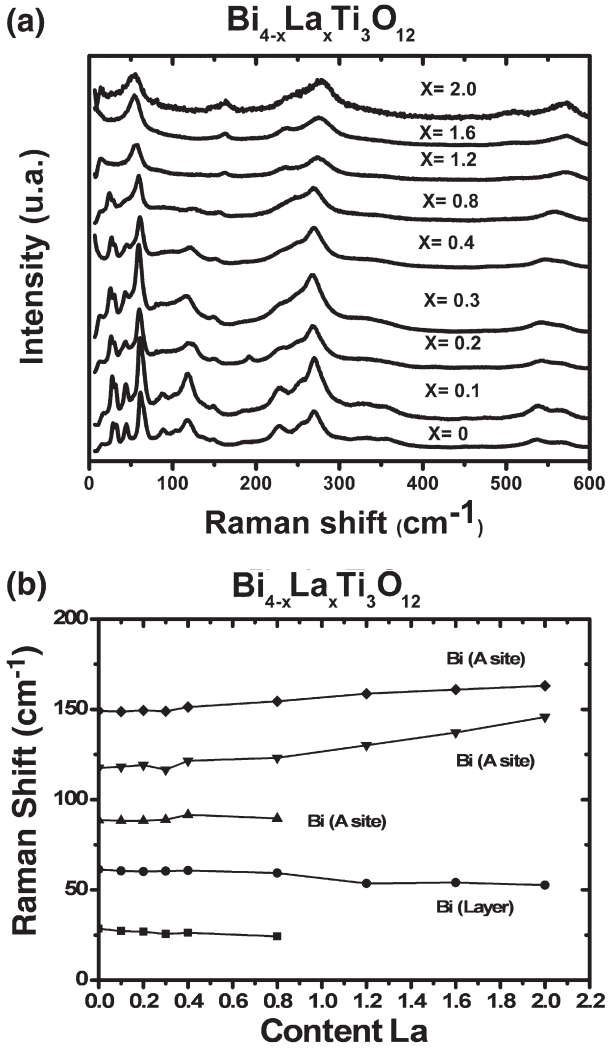

Fig. 1 – (a) Raman spectra of $Bi_{4-x}La_xTi_3O_{12}$ and (b) compositional dependence of the low-frequency modes for $Bi_{4-x}La_xTi_3O_{12}$.

in the pseudoperovskite layer [8]. One particularly important issue is to find where the La^{3+} and Nd^{3+} ions are incorporated and how the doping level influences the structure; an issue which may shed new light on the inherent properties of this material.

Optical phonons are sensitive to variations in interatomic potentials and local site coordination. Atomic substitution can therefore be monitored trough the variations in frequency and intensity of Raman active modes [9].

Osada *et al.* [9] investigated Raman spectra of $Bi_{4-x}La_xTi_3O_{12}$ ($x=0$–2) prepared via solid-state reaction. With La^{3+} doping, the Bi mode corresponding to perovskite *A* site exhibits a substantial hardening, whereas the Bi mode originating from Bi_2O_2 layer is negligibly changed and they have identified a precise cation distribution, which indicates a pronounced site selectivity of La ions for the *A* site for $x \leq 1$.

Many materials undergo abrupt changes in structure or property on heating and, if the material forms a solid solution, the temperature of the change usually varies with composition. The changes, which may be, for example, ferroelectric–paraelectric transitions at the Curie temperature, can usually be studied readily by Differential Scanning Calorimetry (DSC) since most phase transitions have an appreciable enthalpy of transition [10].

Ultra-fine powders with high purity are needed in order to fabricate well-sinterable and phase-pure ferroelectric ceramics. There are several methods to synthesize $Bi_4Ti_3O_{12}$ powders, including solid-state reaction [11], fused salt [12], hydrothermal synthesis [13], sol–gel processing [14], and co-precipitation [15] processes. While most of the studies on tape-cast and sintered platelets reported relative density to be less than 95% of theoretical value [15,16], Villegas *et al.* [17] have used an oxalate co-precipitation method to prepare $Bi_4Ti_3O_{12}$ powder and they have obtained a well-densified ceramic (>97% theoretical density) [18].

In this paper, the Bi_{4-x} $RE_xTi_3O_{12}$ ($RE=La^{3+}$, Nd^{3+}) powders were prepared by a co-precipitation method and characterized by DSC, Raman spectroscopy and XRD. We analyze Raman spectra of $Bi_{4-x}La_xTi_3O_{12}$ and $Bi_{4-x}Nd_xTi_3O_{12}$ within $x=0$ to 2, the ferroelectric–paraelectric transitions and how the La^{3+} and Nd^{3+} ion addition modified the crystal structure.

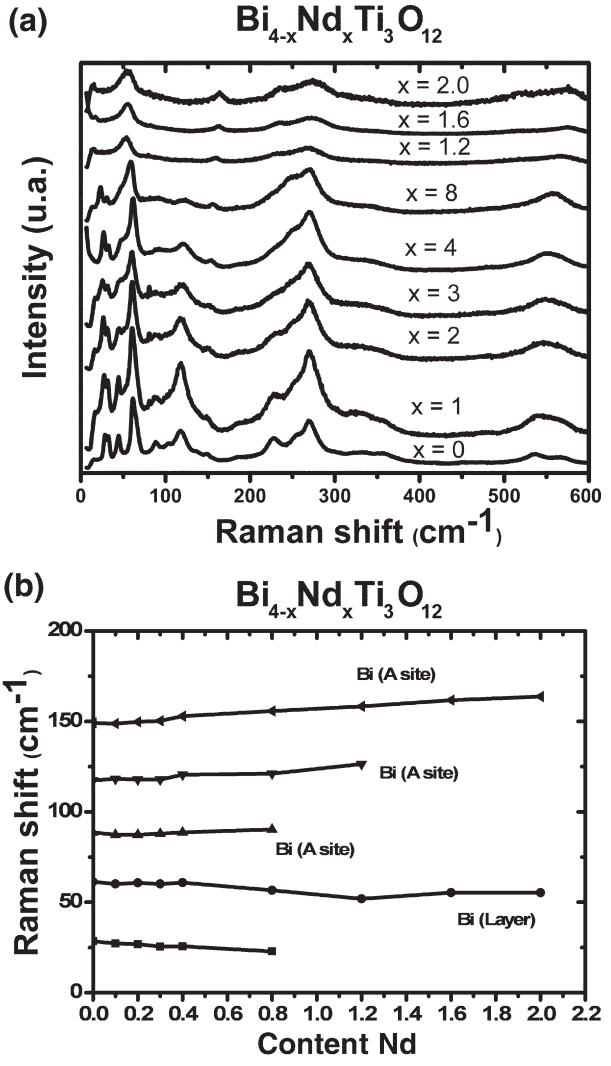

Fig. 2 – (a) Raman spectra of $Bi_{4-x}Nd_xTi_3O_{12}$ and (b) compositional dependence of the low-frequency modes for $Bi_{4-x}Nd_xTi_3O_{12}$.

2. Experimental

$Bi(NO_3)_3{\cdot}5H_2O$ Aldrich 99.99%, $Ti((CH_3)_2CHO)_4$ Aldrich 97% and Nd_2O_3 Ventron 99.9% or $(C_2H_3O_2)_3La{\cdot}H_2O$ Aldrich 99.9%, powders were used as starting materials. First, two solutions were prepared by dissolving $Bi(NO_3)_3{\cdot}5H_2O$ and either Nd_2O_3 or $(C_2H_3O_2)_3La{\cdot}H_2O$ in nitric acid, at pH<2. A third solution was prepared by dissolving $Ti((CH_3)_2CHO)_4$ in a 5/95 vol.% mixture of acid nitric and isopropanol. The three solutions were eventually mixed together and were precipitated using a concentrated ammonia solution under stirring. During the whole process, the pH was maintained above 11. The final precipitate was washed with isopropanol to get a pH of 7, and was dried at 90 °C overnight.

Raman measurements were performed with T64000 instrument from Horiba — Jobin Yvon using the 514.5 nm line from an Ar^+ laser. The scattered light was dispersed by a triple spectrometer with double subtractive stage (spectral resolution<1.5 cm^{-1}). Samples were observed by Scanning Electron Microscopy using a Leica Cambridge Stereo Scan 440 microscope with accelerating 20 kV potential and 500 pA of beam current. Thermal behavior of the as-prepared powder was analyzed by Differential Scanning Calorimetry (DSC) in air in a differential scanning calorimeter TGS-DSC Nestzch, Jupiter STE 449C, with a heating rate of 10 °C/min. The crystalline phase was analyzed by X-ray diffraction (XRD) on annealed powders using a Bruker D8 Advance diffractometer witch uses monochromated CuKα radiation as source.

3. Results and Discussion

3.1. *Cation Distribution in $Bi_{4-x}RE_xTi_3O_{12}$ ($RE=Nd^{3+}$ or La^{3+})*

Figs. 1 and 2 show room-temperature Raman spectra of $Bi_{4-x}La_xTi_3O_{12}$ (BLT) and $Bi_{4-x}Nd_xTi_3O_{12}$ (BNT) exhibiting intense phonons modes at 65, 90, 119, 148, 228, 269, 334, 541 and 616 cm^{-1}. In the ferroelectric phase, the complexity of the BLT and BNT unit cells makes it difficult to assign all observed modes. The activation of "extra" modes is connected either to a strongly distorted structure or oxygen vacancies [9]. The vibrational modes of BIT can be classified as lattice translations involved in Bi^{3+} displacement and internal modes of the TiO_6 octahedron. Considering the vibrational modes related to the atomic mass,

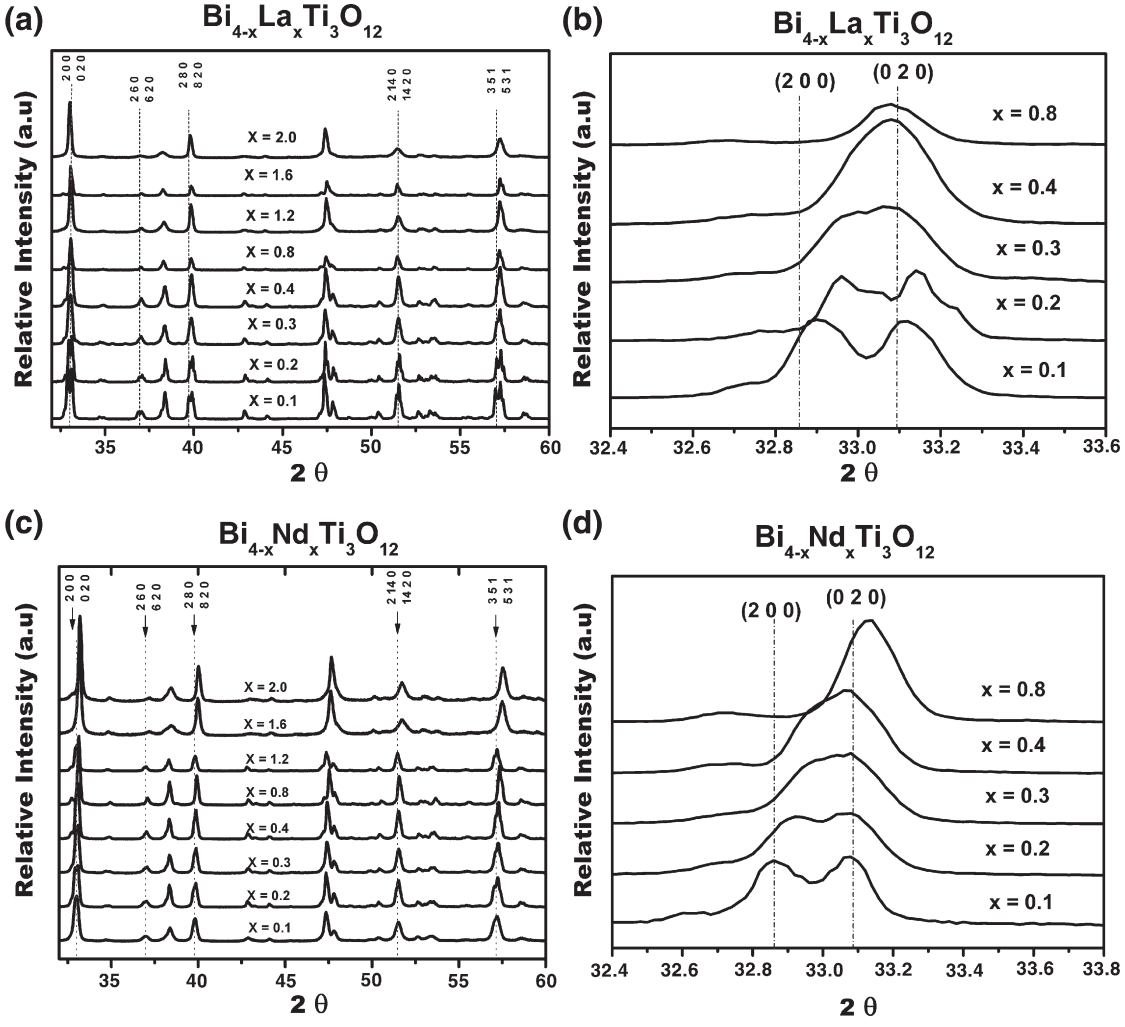

Fig. 3 – (a) and (c) XRD spectrum of BLT and BNT solid solutions, respectively, at several cation concentrations. (b) and (d) XRD spectrum zoom in the peak corresponding [(2 0 0), (0 2 0)] planes for BNT and BLT solid solutions at several cation concentrations.

the low-frequency below 200 cm^{-1} is attributed to the motion of heavy Bi atoms while internal vibrational modes of the TiO_6 octahedron having tree kinds of modes are expected to appear above 200 cm^{-1}. The main bands at ~260, ~460 and ~840 cm^{-1} share a similar doping dependences [9]. The bands below 200 cm^{-1} are attributed to different Bi sites. The band at 65 cm^{-1} is assigned to a rigid-layer mode which originates from Bi displacement in the Bi_2O_2 layers. On the other hand, the three bands at 90, 119, and 148 cm^{-1} are related to the Bi atoms in the pseudoperovskite units [19].

Fig. 1(a) shows the Raman spectra obtained for BLT solid solutions at different concentrations of La^{3+}. The intensity of the vibrational modes decays until they disappear, as what occurs for the band at 90 cm^{-1} due to random distribution of cation in the three possible A sites, replacing Bi^{3+} in the pseudoperovskite lattice [19,20].

Fig. 1(b) shows the wavenumber dependence of the vibrational modes with the amount of La^{3+}. The band at 60 cm^{-1}, which is associated with the Bi^{3+} in the $(Bi_2O_2)^{2+}$ layers is invariant with respect to La^{3+} concentration until $x=1.2$, where small variation appears. This implies that $(Bi_2O_2)^{2+}$ layers do not participate in the substitution process of BLT solid solutions with $x\leq 1.2$. In contrast, the bands at 90, 119 and 148 cm^{-1}, which are associated with the Bi^{3+} in the A sites, get diffuse and their wavenumber increases with the increment of La^{3+} in solid solution, which implies that A site participates actively in the substitution process in the BLT solid solutions with $x\leq 1.2$ [9].

The change in vibrational modes at frequencies greater than 150 cm^{-1} is related with the decrease in the octahedral tilting and the relaxation of lattice distortions. This is indicative of the phase transition of orthorhombic structure to tetragonal structure [20].

Fig. 2(a) and (b) shows the Raman spectra of BNT and the dependence of vibrational modes on the amount of Nd^{3+}, respectively. The behavior observed of vibrational modes in BNT solid solutions is similar to that observed in BLT solid solutions. In BNT solid solutions the band at 60 cm^{-1} is invariant with respect to Nd^{3+} concentration until $x=0.8$. At greater concentrations the vibrational modes are slightly modified. As in BLT solid solutions, it implies that $(Bi_2O_2)^{2+}$ layers participation to the substitution process stars from $x=0.8$ only.

The ionic radii of Bi^{3+} and La^{3+} are almost the same [21], whereas Nd^{3+} is smaller. Consequently, in BNT solid solutions the octahedron formed by oxygen atoms is more distorted than in BLT solid solutions. For this reason, in BNT solid solution the vibrational modes associated with the layers are slightly modified from $x=0.8$ whereas for the vibrational modes in BLT solid solution these modifications are displayed at higher concentration ($x\geq 1.6$).

The influence of the ionic radius of cations is also observed in the X-ray diffraction spectra (XRD). Fig. 3(a) and (c) shows the XRD spectrum of BLT and BNT solid solutions, respectively. Fig. 3(b) shows a peak corresponding to [(2 0 0), (0 2 0)] Bragg reflections at several La^{3+} concentrations. It can be clearly seen from Fig. 3(b) that the shift of peaks in the Bragg's reflections for the BLT as function of La^{3+} concentration is practically zero. Nevertheless, in Fig. 3(d) for the BNT compositions, the shift of the peaks increases as Nd^{3+} concentration increases and for $x=0.8$ the corresponding

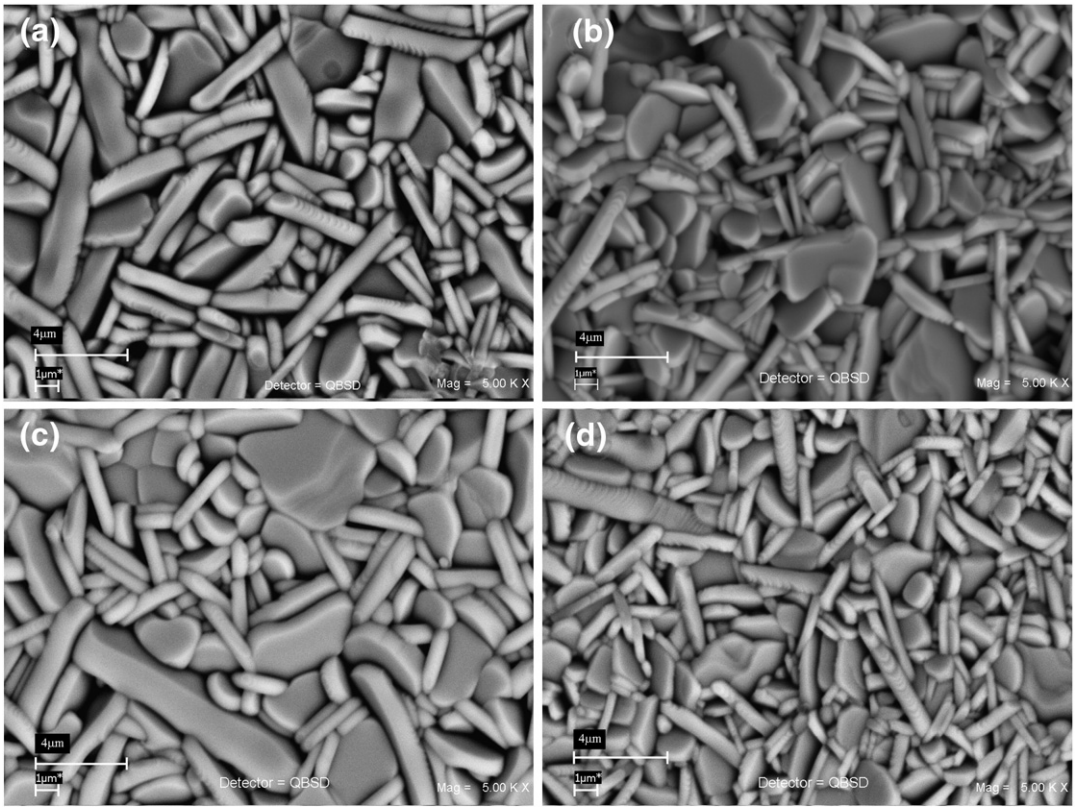

Fig. 4–(a) and (b) SEM micrographs of BLT for $x=0.4$ and 1.2 respectively, (c) and (d) SEM micrographs of BNT for $x=0.4$ and 1.2 respectively.

BNT has a shift of peaks bigger than that for the corresponding BLT.

3.2. Microstructure: SEM Images

Fig. 4(a), (b), (c) and (d) shows SEM micrographs of the sintered BLT and BNT, respectively for x=0.4 and 1.2. The platelet shape morphology is compatible with the synthesis method and the crystal cell of each one of the samples. Actually, these results agree with other studies in similar compounds [22]. All images depict grain size in the order of micrometers, specifically the average for BLT with x=0.4 and 1.2 are 2.9 μm and 3.1 μm respectively, and for BNT with x=0.4 and 1.2 are 3.0 μm and 2.5 μm, respectively. For the different samples the average grain size doesn't follow any correlation between them. The effect on the shape and band maxima of Raman spectra [23] when the grain size is in the order of nanometers is well established, but as we mentioned above the samples used for this study do not match this condition, thus the shift and shape modification of Raman spectrum bands in BLT and BLN series are induced by the progressive substitution of Bi^{3+} for La^{3+} or Nd^{3+} and the site where they are placed.

3.3. Curie Temperature Dependence

The ferroelectric to paraelectric phase transition was followed by DCS as a function of the doping fraction in BLT and BNT. The experimental curves as well as Curie temperature *vs.* doping fraction plots are given in Fig. 5. Wolfe and Newnham proposed the following linear relationship for $Bi_{4-x}RE_xTi_3O_{12}$ compounds [24].

$$T_c = 669 - M\left(r_{RE}^{3+} - r_{Bi}^{3+}\right)(x) \quad \text{where } M \text{ is a constant.} \tag{1}$$

Linear adjustments to our curves lead to the following results

$$Tc_{BLT\ solid\ solution} = 669 - 443(x) \quad R^2 = 0.9954. \tag{2}$$

$$Tc_{BNT\ solid\ solution} = 669 - 300(x) \quad R^2 = 0.9883 \tag{3}$$

where *x* is the cation amount in the BLT and BNT solid solutions.

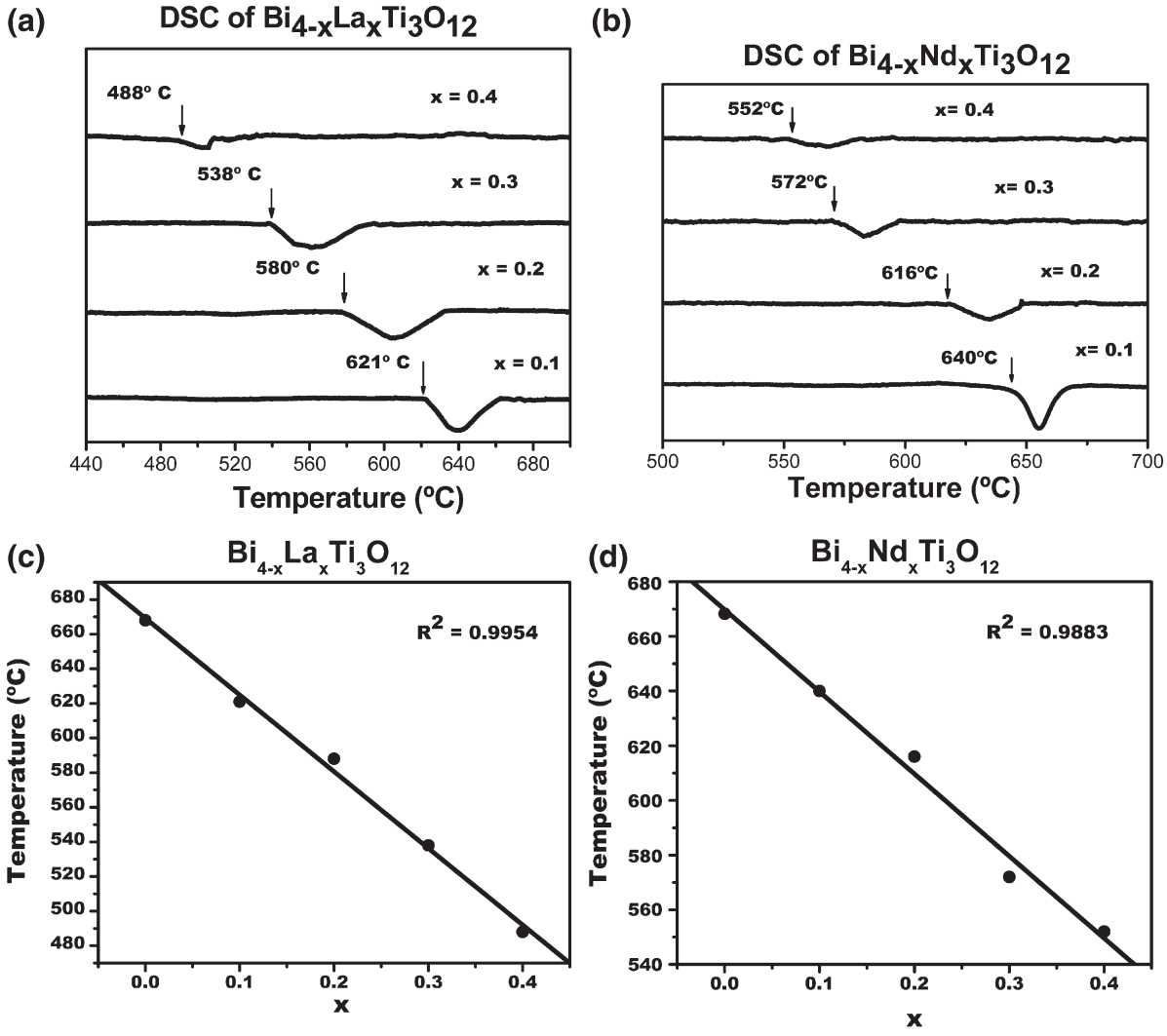

Fig. 5 – (a) and (b) DSC thermograms of BLT and BNT respectively for different concentrations, (c) and (d) the linear adjustment of T_c.

Whit r_{La}^{3+}=1.14 Å and r_{Bi}^{3+}=0.83 Å and r_{Nd}^{3+}=1.04 Å [25], Eqs. (2) and (3) return the same *M* value of 1429. In Eq. (1), BLT and BNT thus obey the following law:

$$Tc = 669 - 1429\left(r_{ER}^{3+} - r_{Bi}^{3+}\right)(x). \quad (4)$$

The addition of La^{3+} or Nd^{3+} into solid solution in the BIT lattice diminishes the distortion in the octahedra formed by oxygen atoms, making *a* and *b* parameters closer. When they get equal, a change in crystal structure from orthorhombic to tetragonal is produced, this increment of symmetry is associated with the transition of ferroelectric to paraelectric behavior. When increasing the amount of the cation, the system requires less energy to make this change of symmetry, this is the reason thus T_c diminishes based on the amount of cation in the BIT.

4. Conclusions

By means of Raman spectroscopy it was observed that La cations were placed preferentially in *A* sites in concentrations $x \leq 1.2$ and for greater concentrations, evidence of presence of La cations was observed as much in A sites as in the $(Bi_2O_2)^{2+}$ layers. The Nd cations have a similar behavior in the solid solutions, Nd cations are placed preferentially in *A* sites for concentration $x \leq 0.8$, whereas for concentrations $x > 0.8$ evidence of presence of Nd cations is observed as much in *A* sites as in the $(Bi_2O_2)^{2+}$ layers. We discard the grain size effect on the Raman Spectra by Scanning Electron Microscopy.

La^{3+} and Bi^{3+}ionic ratios are very similar. Nevertheless, Nd^{3+} ionic radius is smaller than the very close La^{3+} and Bi^{3+} ionic radii. For this reason the solid solution limit for $Bi_{4-x}Nd_xTi_3O_{12}$ is smaller than in the solid solution $Bi_{4-x}La_xTi_3O_{12}$.

As observed using X-ray diffraction La^{3+} atoms in BLT solid solutions generate a subtle peak diffraction shifts, as well as, Nd^{3+} cations in BNT solid solution the peak diffraction shifts are evident.

The Curie temperature is linearly dependent on the amount of cation present in the solid solution, and the slope is a function of ionic ratios of Bi^{3+}, Nd^{3+} and La^{3+}. We used the model proposed by Wolfe and Newnham with the parameter *M*=1429 calculated by us, in order to describe the Curie's temperature behavior in this kind of solid solutions.

Acknowledgements

Authors would like to thank CONACyT-SEP-2004-CO1-47541, DGAPA UNAM IN103603 for financial support and DGAPA UNAM for sabbatical sponsor. The authors are grateful to L. Baños and M.A. Cortés for technical support.

REFERENCES

[1] Aurivillius B. Ark Kemi 1949;1:499.
[2] Dorrian JF, Newnham RE, Smith DK, Kay MI. Crystal structure of Bi_4 Ti_3 O_{12}. Ferroelectrics 1971;3:17–27.
[3] Shimakawa Y, Kubo Y, Tauchi Y, Asano H, Kamiyama T, Izumi F, et al. Crystal and electronic structures of $Bi_{4-x}La_xTi_3O_{12}$ ferroelectric materials. Appl Phys Lett 2001;79:2791–3.
[4] Watanabe T, Kojima T, Sakai T, Funakubo H, Osada M, Noguchi Y, et al. Large remanent polarization of $Bi_4Ti_3O_{12}$-based thin films modified by the site engineering technique. J Appl Phys 2002;92:1518–21.
[5] Park BH, Kang BS, Bu SD, Noh TW, Lee J, Jo W. Lanthanum-substituted bismuth titanate for use in non-volatile memories. Nature 1999;401:682.
[6] Sun YM, Chen YC, Gan JY, Hwang JC. Ferroelectric properties of (117)- and (001) oriented $Bi_{3.25}La_{0.75}Ti_3O_{12}$ polycrystalline thin films. Appl Phys Lett 2002;81:3221–3.
[7] Li W, Su D, Zhu J, Wang Y. Mechanical and dielectric relaxation in neodymium modified bismuth titanate ceramics. Solid State Commun 2004;131:189–93.
[8] Rae AD, Thompson JG, Withers RL, Willis AC. Structure refinement of commensurately modulated bismuth titanate, $Bi_4Ti_3O_{12}$. Acta Crystallogr Sect B Struct Sci 1990;46:474–87.
[9] Osada M, Tada M, Kakihana M, Watanabe T, Funakubo H. Cation distribution and structural instability in $Bi_{4-x}La_xTi_3O_{12}$. Jpn J Appl Phys 2001;40:5572–5.
[10] West AR. Solid state chemistry and its applications. New York: Wiley; 1998.
[11] Van Uiter LG, Egerton L. Bismuth titanate. A Ferroelectric J Appl Phys 1961;32:959.
[12] Timura T, Kanazawa T, Yamaguchi T. Two-mode behavior in complex perovskite materials. J Am Ceram Soc 1989;72:158–60.
[13] Chen DR, Jiao XL. Hydrothermal synthesis and characterization of $Bi_4Ti_3O_{12}$ powders from different precursors. Mater Res Bull 2001;36:355.
[14] Prasada Rao AV, Robin AI, Kormaneni S. Bismuth titanate from nanocomposite and sol–gel processes. Mater Lett 1996;28:469–73.
[15] Xiang PH, Kinemuchi Y, Nagaoka T, Watari K. Sintering behaviors of bismuth titanate synthesized by a coprecipitation method. Mater Lett 2005;59:3590–4.
[16] Swarts S, Schulze WA, Biggers JV. Fabrication and electrical properties of grain oriented ceramics $Bi_4Ti_3O_{12}$. Ferroelectrics 1981;38:765–8.
[17] Villegas M, Moure C, Fernandez JF, Duran P. Preparation and sintering behaviour of submicronic $Bi_4Ti_3O_{12}$ powders. Mater Sci 1996;31:949–55.
[18] Kan Y, Wang P, Li Y, Cheng YB, Yan D. Low-temperature sintering of $Bi_4Ti_3O_{12}$ derived from a co-precipitation method. Mater Lett 2002;56:910–4.
[19] Jeon MK, Kim Y, Shon JM, Woo SI. Cation disorder study of $Bi_{3.25}La_{0.75}Ti_3O_{12}$ by neutron powder diffraction and Raman spectroscopy. J Phys D Appl Phys 2004;37:2588–92.
[20] Wang Y, Zhang X, Feng Y, Tang W, Cheng G, Zhu Y. Structural and optical properties of $Bi_{4-x}Nd_xTi_3O_{12}$ thin films prepared by metal-organic solution deposition. Mater Lett 2004;58:813–6.
[21] Shannon RD. Revised effective ionic radii and systematic studies of interatomic distances in halides and chalcogenides. Acta Crystallogr 1976;A 32:751–67.
[22] Villafuerte-Castrejón M, Camacho-Alanís F, González F, Ibarra-Palos A, González G, Fuentes L, et al. Luminescence and structural study of $Bi_{4-x}Eu_xTi_3O_{12}$ solid solution. J Eur Ceram Soc 2007:545–9.
[23] Gouadec G, Colomban P. Raman Spectroscopy of nanomaterials: how spectra relate to disorder, particle size and mechanical properties. Prog Cryst Growth Charact Mater 2007;53:1–56.
[24] Wolfe RW, Newnham RE. Rare-earth bismuth titanates. J Electrochem Soc 1969;116:832–5.
[25] Arhens LH. The use of ionizations potentials. Part 1 Ionic radii of elements. Geochim Cosmochim acta 1952;2:155–69.